CHARACTERIZATION OF ADHESION BETWEEN DISSIMILAR POLYMER-MATRIX COMPOSITES

Diana G. Heflin[1,2], Joshua Dustin[2], Jan-Anders E. Mansson[1,2]

[1]School of Materials Engineering, Purdue University
701 W Stadium Ave.
West Lafayette, IN 47907

[2]Composites Manufacturing and Simulation Center
1105 Challenger Ave., Suite 100
West Lafayette, IN 47906

ABSTRACT

Epoxy-matrix composites are highly brittle and tend to fail catastrophically, which can be dangerous and costly. Therefore an area of great potential in composite manufacture is improving the toughness—that is, the energy absorption ability, of the polymer matrix. Including a second, less brittle polymer phase can increase the toughness of a composite, in turn enhancing the damping and impact energy absorption. In order to take full advantage of these enhanced properties, the adhesion must be sufficient that an applied load can be transferred between the two phases without causing adhesive failure. Adhesion behavior between epoxy and polyamide 6 elastomer is examined for compression molded samples using the wedge test. The influence of processing conditions on adhesion is also investigated. The strength of the bonds suggests that these matrix combinations provide viable avenues for toughening existing composite materials.

1. INTRODUCTION

As composites become more widely used for a wider range of applications, there is great interest in enhancing their mechanical properties and processability. Current high-performance epoxy-matrix composites tend to be brittle with poor high- and low- velocity impact performance. Though lower impact rates may not result in failure, parts made from such composites have poor damping characteristics, often resulting in poor feel and control for the consumer. Therefore, an area of great potential in composites is improving the energy absorption ability of the polymer matrix.

Based on principles of good adhesion and effective epoxy toughening, polyamide (PA) is an ideal candidate to serve as a toughening agent. The amide groups are able to react to form strong covalent bonds with epoxy, and both epoxy and PA are polar molecules. This compatibility enhances their miscibility, promoting interdiffusion to allow for mechanical as well as chemical crosslinking. Further, as a semicrystalline polymer, PA is stiff enough to limit debonding at the interface due to a mismatch in material properties, yet ductile enough to provide damping to epoxy matrices.

SAMPE Conference Proceedings. Charlotte, NC, May 20-23, 2019. Society for the Advancement of Material and Process Engineering – North America.

PA has been successfully incorporated into epoxy-matrix composite systems in various geometries including as discrete fibers [1-3], interlayers between composite plies [4-12], and particles in the epoxy matrix [13-15]. In each of these geometries, the PA had the ability to improve the impact energy absorption, reduce impact damage, and improve the mode-I and mode-II fracture toughnesses over composites that did not contain PA. These changes in properties rely on the ability of the PA-epoxy interface to withstand the applied stress and hold the hybrid part intact. In systems where the interface is not sufficiently strong, stress transfer across the interface is not possible and the system cannot benefit from the addition of the PA.

In some cases, however, the performance of a PA-reinforced system was limited by a PA-epoxy bond that was too strong [1, 16, 17]. For systems that must withstand large applied loads, PA delamination and subsequent deformation are valuable energy absorption mechanisms. If the bond between the polymers is too strong, the PA phase cannot deform to its full extent and its contribution to the impact energy absorption is limited. Therefore, neither stronger nor weaker interfaces are inherently better, as either may be appropriate for a given performance target.

The goal of this work is to quantify the adhesion between epoxy and PA matrices, as well as to determine the effect of processing on adhesive strength. The strength of the interface between the two polymer phases is a primary factor that determines the mechanical properties of a part made from a hybrid composite. Therefore, adjusting the bond strength via the processing parameters could allow for tuning of macroscale mechanical properties.

2. EXPERIMENTATION

2.1 Materials

Two different polymer-matrix pre-impregnated composite materials (prepregs) were used. The first was a unidirectional glass fiber (GF) prepreg with a polyamide 6 (PA6) matrix from Plasticomp. The PA6 prepreg was dried before each processing step to eliminate water from the hydrophilic PA6. $[0]_{14}$ layups of the PA6/GF prepreg were pre-consolidated at 260 ºC and 690 kPa for 10 minutes to create fully consolidated PA6/GF plates.

The second material was a unidirectional carbon fiber (CF) prepreg with a toughened epoxy matrix, CYCOM 977-2. Before combining with other materials, squares of prepreg were laid up using a $[0]_{22}$ layup scheme. Epoxy/CF layups remained uncured until the test plates were manufactured, allowing the epoxy to interact with the other material before curing.

In order for the bending in each half of the beam to be roughly symmetric, the flexural rigidity in each material must be the same. Flexural rigidity depends on the elastic modulus of the material and the sample geometry. In this case, where the material selections have already been made, modifications to flexural rigidity must come from modifications in sample thickness. Sample thicknesses and layups were chosen to minimize the difference in flexural rigidity on either side of the bi-material interface.

Samples were made containing two of the above prepreg layups to assess the adhesion between the dissimilar polymers. A set of samples were also made where material 1 and material 2 were the same to provide a point of comparison.

2.2 Manufacturing Methods

254 mm x 254 mm square plates were manufactured using compression molding under 690 kPa of pressure. A 25.4 mm wide strip of polyimide film was placed along one edge of the mold at the interface, perpendicular to the fiber layup direction. The polyimide does not react with the prepreg matrices, resulting in a non-bonded region along one end of the square plate. This region served as a crack initiation site during testing. The plates were cut into 25.4mm wide strips perpendicular to the polyimide strip to make samples for testing.

Plates were pressed under two different processing times and temperatures to determine the effects of processing conditions on adhesion. The lower temperature was chosen to be the recommended processing temperature for the epoxy/CF prepreg, 177 ºC (350 ºF), and samples were held at temperature for the manufacturer-recommended 3 hours. Plates were also pressed at 197 ºC for 45 minutes—for each 10 ºC increase in temperature, the processing time was cut in half. The plates made from only the PA6/GF prepreg did not adhere to under these processing conditions, so these plates were processed above the PA6 melting temperature to produce usable samples. A summary of the samples, along with the sample IDs used in this paper, is contained in table 1.

Table 1. Sample IDs and processing conditions.

Material 1	Material 2	177 ºC, 3 hr	197 ºC, 45 min	240 ºC, 40 min	260 ºC, 10 min
PA6/GF	PA6/GF			PP240	PP260
Epoxy/CF	Epoxy/CF	EE177	EE197		
PA6/GF	Epoxy/CF	EP177	EP197		

2.3 Experimental Procedure

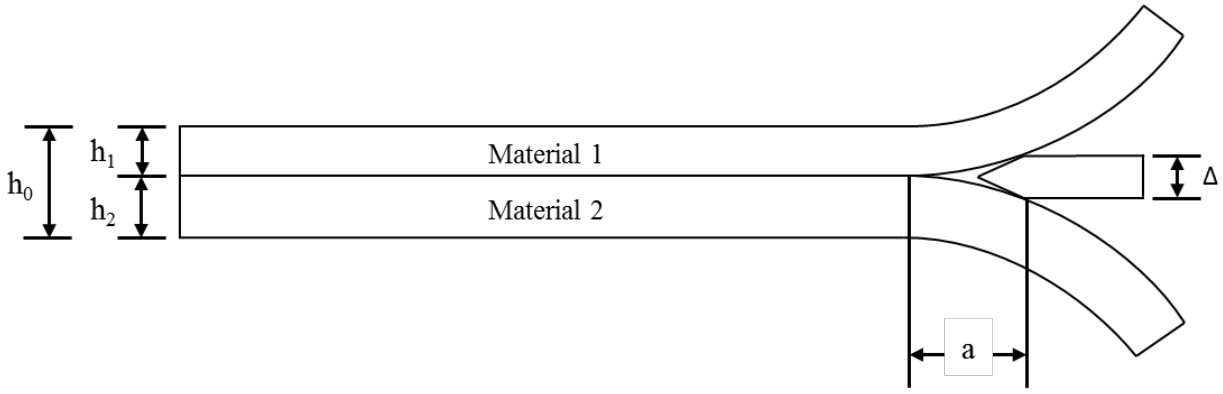

Figure 1. Asymmetric wedge test setup used.

A wedge test setup based on ASTM D3762 [18] was used to assess the mode I interfacial fracture toughness of the samples. A 0.52 mm thick razor blade was inserted into the samples at the interface. The samples were left at ambient conditions until the crack length reached an equilibrium length and stopped growing. The crack tip was determined to be the point along the sample where the total sample thickness deviated from the nominal value h_0. The equilibrium crack length, *a*,

was measured from the crack tip to the point of contact between the razor blade and the sample arms, as shown in figure 1. After crack length measurement, the razor blade was advanced farther into the sample and the test was repeated. This allowed several fracture toughness measurements to be taken along the length of each sample.

Mode I interfacial fracture toughness (G_I) was calculated using equation 1, from Cognard [19]

$$G_1 = \frac{3\Delta^2(E_1 h_1^3 + E_2 h_2^3)}{32a^4} \quad [1]$$

Once the razor blade was advanced to the center of the samples, the testing was stopped and the wedge was removed. Hinges were attached to the top and bottom of the samples and the two halves were pulled the rest of the way apart, resulting in fracture surfaces that were not affected by the razor blade. These neat fracture surfaces were examined using scanning electron microscopy (SEM) to further characterize the failure modes.

3. RESULTS

3.1 Fracture Toughness

There was significant variation in interfacial fracture toughness results between samples. Since all of the samples for a given material combination and set of processing conditions came from a single composite plate, there should be no processing variations between samples from the same plate. Some of the variation may be due to the test method, as even small inaccuracies in the measured crack length could have a large impact on the calculated G_I value.

Despite these large sample-to-sample variations in fracture toughness, meaningful conclusions can still be drawn from the data. Due to the length of the samples, the wedge test was repeated many times per sample, yielding large sample populations that allow for statistical differentiation between the mean values. All of the reported sample means are statistically different from one another.

3.1.1 Effect of processing temperature

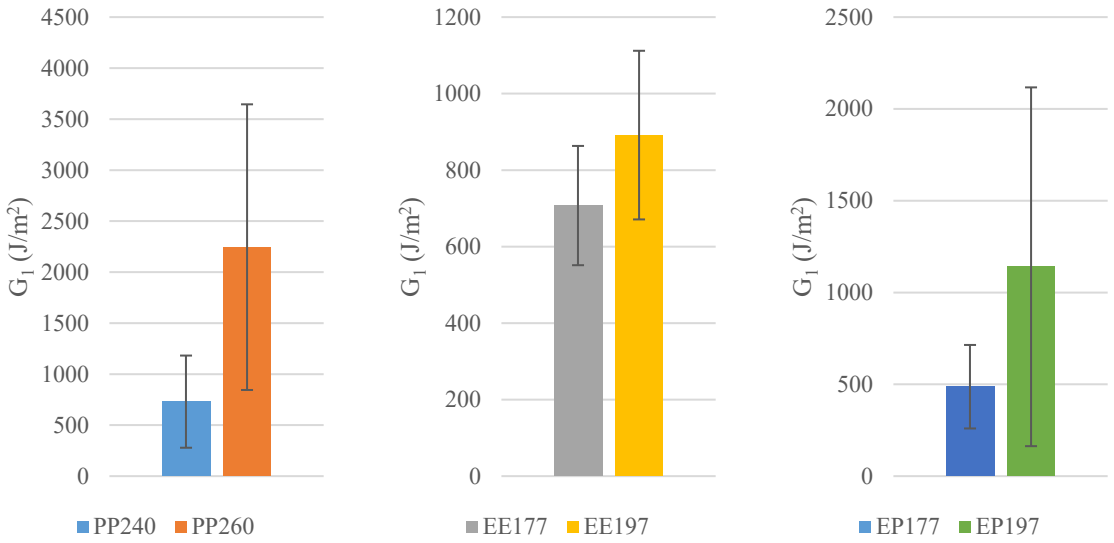

Figure 2. Average interfacial fracture toughness of samples with respect to temperature.

For all material combinations, the plates that were processed at higher temperatures exhibited stronger interfacial fracture toughnesses than the same combination of materials processed at lower temperatures. Figure 2 shows the average G_1 values for each material combination and set of processing conditions. It is likely that the interfacial fracture toughness will reach a maximum value as processing temperature is further increased, because eventually the processing time will become too short for polymer chains to diffuse and interact with the material on the other side of the interface. The epoxy will also begin to cure too quickly, preventing interaction across the interface.

Both PP260 and PP240 were processed above the PA6 melting temperature of 220 ºC, but there is still a significant difference in the resulting G_1 values. The PP240 plates exhibited little to no fiber bridging across the interface, while the PP260 samples had a high degree of fiber bridging. This difference in fracture toughness and failure mode suggests that at the higher processing temperature, the PA6 chains are more free to move and interact across the plate interface.

Though the difference between G_1 as a result of different processing conditions is less extreme in the EE177 and EE197, it is still clear that the higher processing temperature leads to stronger bonding. This is interesting to note, as the lower temperature was the manufacturer-recommended processing condition for the epoxy.

Even though both EP/PA plates were processed below the PA6 melt temperature of 220 ºC, there is still a clearly visible improvement in interfacial fracture toughness with the increase in processing temperature. Some of this improvement may come from the decrease in viscosity of the epoxy at the elevated temperature, but it is also possible that the higher temperature allows for increased PA6 chain mobility in the solid PA6, allowing for more interaction between the epoxy and PA6 chains.

3.1.2 ***Comparison between different material combinations***

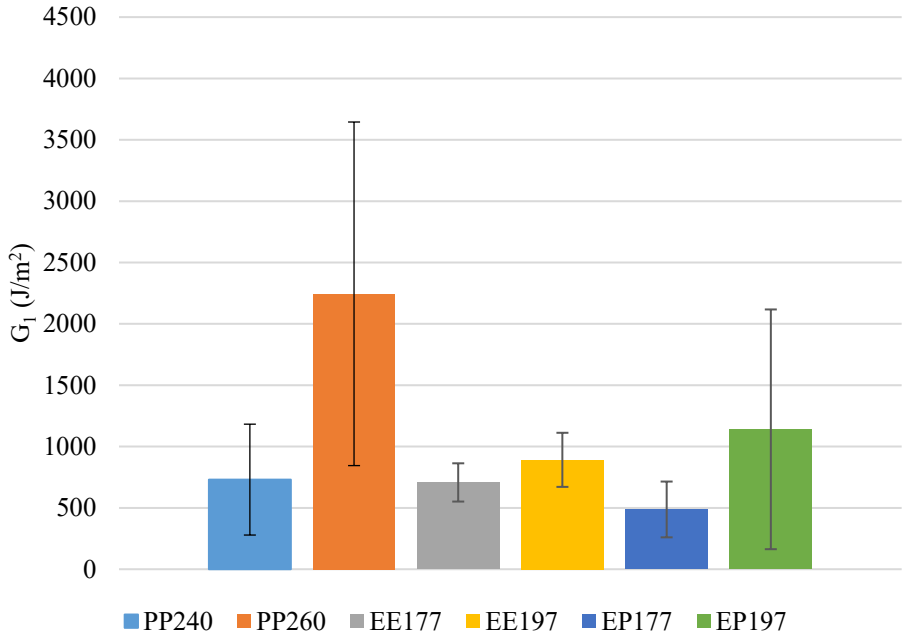

Figure 3. Average G_I values for all material combinations.

The interfacial fracture toughness was greatest in the PP260 samples. The relatively ductile PA6 matrix is able to dissipate a large amount of energy, resulting in matrix deformation relatively far from the interface that allows the material to support a greater interface load. This energy absorption mechanism is available to all PA6-containing samples provided that the interface is strong enough to withstand the applied load long enough to transfer the load to the PA6 matrix. In PA6-containing samples where the interfacial bond was not sufficiently strong, the two beams separated before energy could be transferred away from the interface. Therefore, it is essential that the processing conditions allow the bond strength to be sufficiently strong to the load away from the interface.

The EP197 interfaces are stronger than both the EE177 and EE197 interfaces, so the presence of the PA6 enhanced the mode I behavior over the neat epoxy matrix. As the cracks extended through the EP197 samples, the PA6 matrix began to fail cohesively, away from the epoxy/PA6 interface. This suggests that improving bonding at the interface may not improve part performance in mode I testing, as the bonding at the interface was stronger than the bulk PA6/GF material.

3.2 **Microscopy**

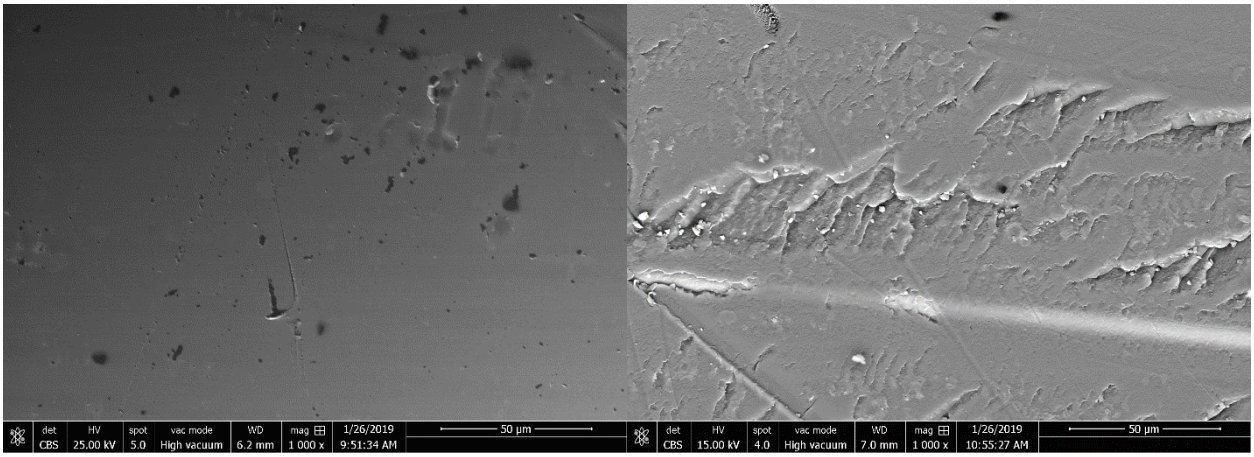

Figure 4. SEM images of PA6/GF fracture surfaces from EP 177(left) and EP197 (right) samples at 1000x magnification.

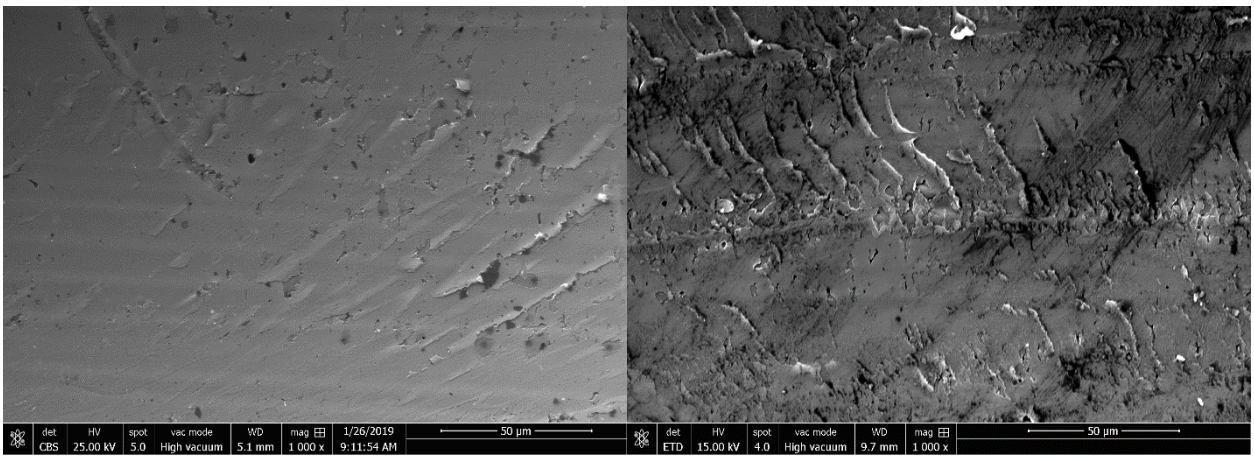

Figure 5. SEM images of epoxy/CF fracture surfaces from EP 177(left) and EP197 (right) samples at 1000x magnification.

EP177, has a neat, planar fracture surface with little evidence of interaction between the epoxy and PA6 matrices. EP197, on the other hand, has plastic deformation in the both the epoxy and the PA6 matrices, as well as signs of cohesive failure in the PA6 near the fracture surface. This is an indication that the local bond between the epoxy and the PA6 near the fracture surface was sufficiently strong to drive the crack growth into the PA6 matrix. Neither hybrid sample appears to have interaction between the two halves of the samples beyond the matrix-rich region right at the interface, as indicated by the lack of bare fibers on the fracture surfaces. This could be due to several factors, including the disparate sizes of the reinforcing fibers and the fact that the processing temperatures were below the PA6 melting temperature, limiting fiber mobility within the PA6 matrix.

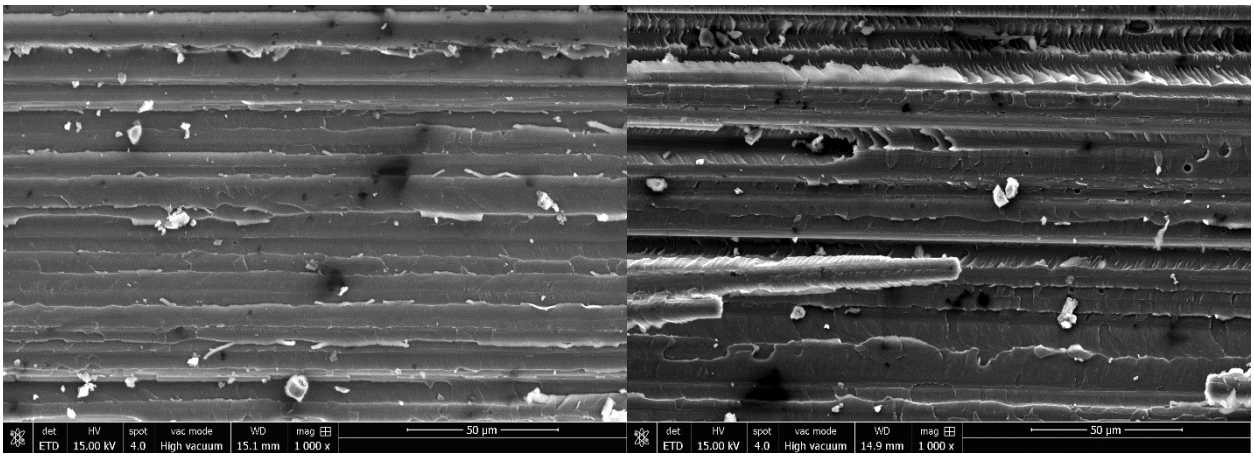

Figure 6. SEM images of fracture surfaces of EE177 (left) and EE197 (right) samples at 1000x magnification.

The EE197 sample has regions of plastic deformation, visible in the upper right corner of the SEM image. The EE177 sample, which had lower measured interfacial fracture toughness, has less visible plastic deformation in the matrix, indicating that matrix plastic deformation may play a role in improving fracture toughness. Both samples have some fiber breakage at the interface, but the damage is largely confined to the resin-rich region.

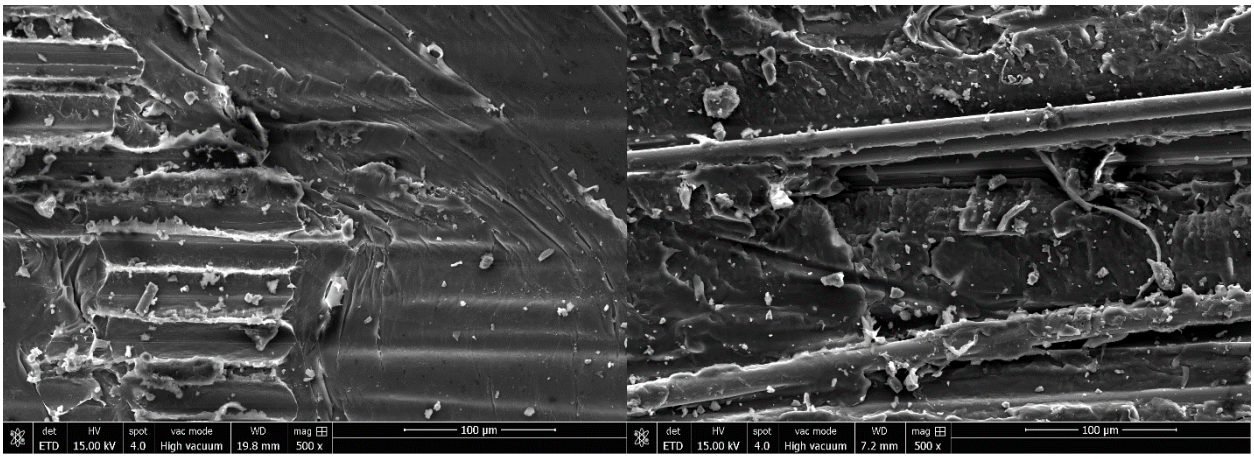

Figure 7. SEM images of fracture surfaces of PP240 (left) and PP260 (right) at 500x magnification.

Though both PP240 and PP260 appear to have a large degree of plastic deformation in the PA6 matrices based on the SEM images, the damage in the PP240 sample seems largely superficial, with large areas of largely intact PA6 matrix still covering the glass fibers (as on the right side of the image) . This indicates that the bonding between the two halves on the sample was confined to a shallow region around the interface. By contrast, the PP260 sample has multiple visible layers of glass fibers and deformed PA6 matrix, suggesting that the damage zone (and, by extension, the bonded region) extended deeper into the sample, away from the immediate vicinity of the interface.

Perhaps the greater bond strength in the PP260 sample can be partially attributed to this larger interface region.

Based on the SEM images of the fracture surfaces, surface roughness does not appear to be the only factor in determining interfacial fracture toughness, as the EP197 sample has a relatively smooth fracture surface compared to the EE and PP samples, yet it has one of the highest G_I values. It seems that the interfacial failure mechanism depends greatly on the material system. However, the apparent depth of the damaged interface region, the degree of plastic deformation, and the amount of fiber breakage and pullout can give an indication of the expected relative G_I values for samples with the same combination of materials.

4. CONCLUSIONS

It has been shown that the bond between compression molded epoxy and PA6 is sufficiently strong to create an interface that is stronger than the neat epoxy-epoxy interface. This strong bond was achieved without any surface pretreatments on either polymer matrix, making this combination of polymers well-suited for manufacturing processes that require efficiency and few processing steps.

There is a clear dependence of bond strength on processing temperature, particularly for samples that include PA6. At higher temperatures, the PA6 chains are increasingly mobile and able to interact with epoxy and PA6 chains across the interface.

It is worth noting that the epoxy matrix used in this study has a relatively long cure cycle. Even when the cure time is decreased with higher processing temperature, there is still ample time for polymer chains to interact across the interface. Faster-curing epoxies may not exhibit an increase in interfacial fracture toughness with increasing processing temperature, as the cure time may be insufficient for mechanical and chemical interlocking to occur.

Future work will examine the effect of combining composites with disparate polymer matrices on mechanical properties including impact energy absorption and fatigue, as well as the effect of interfacial bond strength on the resultant macroscopic properties of such composites. Further, double cantilever beam (DCB) tests will be conducted to validate and provide a comparison with G_I values determined using the wedge test.

5. REFERENCES

1. Jang, B.Z., et al. “Impact Resistance and Energy Absorption Mechanisms in Hybrid Composites.” *Composites Science and Technology* 34 (1989): 305-335. http://doi.org/10.1016/0266-3538(89)90002-X.
2. Beier, Uwe, et al. “Mechanical Performance of Carbon Fibre-Reinforced Composites Based on Preforms Stitched with Innovative Low-Melting Temperature and Matrix Soluble Thermoplastic Yarns.” *Composites Part A: Applied Science and Manufacturing* 39(9) (2008): 1572–1581. http://doi.org/10.1016/j.compositesa.2008.06.003.

3. Hogg, Paul J. “Toughening of Thermosetting Composites with Thermoplastic Fibres.” *Materials Science and Engineering: A* 412 (2005): 97–103. http://doi.org/10.1016/j.msea.2005.08.028.
4. Favre, Jean-Paul. “Improving the Fracture Energy of Carbon Fibre-Reinforced Plastics by Delamination Promoters.” *Journal of Materials* Science 12 (1977): 43-50. http://doi.org/10.1007/BF00738470.
5. Masters, John E. “Improved Impact and Delamination Resistance through Interleafing.” *Key Engineering Materials*, 37 (1989): 317–348. http://doi.org/10.4028/www.scientific.net/kem.37.317.
6. Daelemans, Lode, et al. “Using Aligned Nanofibres for Identifying the Toughening Micromechanisms in Nanofibre Interleaved Laminates.” *Composites Science and Technology* 124 (2016): 17–26. http://doi.org/10.1016/j.compscitech.2015.11.021.
7. Daelemans, Lode, et al. “Damage-Resistant Composites Using Electrospun Nanofibers: A Multiscale Analysis of the Toughening Mechanisms.” *ACS Applied Materials & Interfaces*, 8(18) (2016): 11806–11818. http://doi.org/10.1021/acsami.6b02247.
8. Akangah, Paul, et al. “Effect of Nylon-66 Nano-Fiber Interleaving on Impact Damage Resistance of Epoxy/Carbon Fiber Composite Laminates.” *Composite Structures* 92(6) (2010): 1432–1439. http://doi.org/10.1016/j.compstruct.2009.11.009.
9. Palazzetti, R., et al. “The Self-Reinforcing Effect of Nylon 6,6 Nano-Fibres on CFRP Laminates Subjected to Low Velocity Impact.” *Composite Structures* 106 (2013): 661–671. http://doi.org/10.1016/j.compstruct.2013.07.021.
10. Palazzetti, R., et al. “Influence of Electrospun Nylon 6,6 Nanofibrous Mats on the Interlaminar Properties of Gr–Epoxy Composite Laminates.” *Composite Structures* 94(2) (2012): 571–579. http://doi.org/10.1016/j.compstruct.2011.08.019.
11. Tsotsis, Thomas K. “Interlayer Toughening of Composite Materials.” *Polymer Composites* (2009): 70–86. http://doi.org/10.1002/pc.20535.
12. Daelemans, Lode, et al. “Nanofibre Bridging as a Toughening Mechanism in Carbon/Epoxy Composite Laminates Interleaved with Electrospun Polyamide Nanofibrous Veils.” *Composites Science and Technology* 117 (2015): 244–256. http://doi.org/10.1016/j.compscitech.2015.06.021.
13. Groleau, M.R., et al. “Mode II Fracture of Composites Interlayered with Nylon Particles.” *Composites Science and Technology* 56(11) (1996): 1223–1240. http://doi.org/10.1016/s0266-3538(96)00080-2.
14. Caprino, G., et al. “The Effect of Shear on the Rigidity in Three-Point Bending of Unidirectional CFRP Laminates Made of T800H/3900-2.” *Composite Structures* 88(3) (2009): 360–366. http://doi.org/10.1016/j.compstruct.2008.04.014.
15. Hojo, Masaki, et al. “Mode I Delamination Fatigue Properties of Interlayer-Toughened CF/Epoxy Laminates.” *Composites Science and Technology* 66(5) (2006): 665–675. http://doi.org/10.1016/j.compscitech.2005.07.038.
16. Cardwell, B.J. and Yee, A.F. “Toughening of Epoxies through Thermoplastic Crack Bridging.” *Journal of Materials Science* 33 (1998): 5473-5484. http://doi.org/10.1023/A:1004427123388.

17. Thanomsilp, C. and Hogg, P.J. “Penetration Impact Resistance of Hybrid Composites based on Commingled Yarn Fabrics.” *Composites Science and Technology* 63 (2003): 467-482. https://doi.org/10.1016/S0266-3538(02)00233-6

18. ASTM Standard D3762-03, 2010, “Standard Test Method for Adhesive-Bonded Surface Durability of Aluminum (Wedge Test)” ASTM International, West Conshohocken, PA, 2010, DOI: 10.1520/D3762-03R10, www.astm.org

19. Cognard, J. “The Mechanics of the Wedge Test.” *The Journal of Adhesion* 20(1) (1986): 1-13. http://doi.org/10.1080/00218468608073236.